ACE OBSERVATIONS OF THE BASTILLE DAY 2000 INTERPLANETARY DISTURBANCES

C. W. SMITH[1], N. F. NESS[1], L. F. BURLAGA[2], R. M. SKOUG[3], D. J. MCCOMAS[4],
T. H. ZURBUCHEN[5], G. GLOECKLER[5,6], D. K. HAGGERTY[7], R. E. GOLD[7],
M. I. DESAI[6], G. M. MASON[6,8], J. E. MAZUR[9], J. R. DWYER[10], M. A. POPECKI[11],
E. MÖBIUS[11], C. M. S. COHEN[12] and R. A. LESKE[12]

[1]*Bartol Research Institute, University of Delaware, Newark, Delaware 19716, U.S.A*
[2]*Code 692, NASA/Goddard Space Flight Center, Greenbelt, MD 20771, U.S.A.*
[3]*Los Alamos National Laboratory, Los Alamos, NM 87545, U.S.A.*
[4]*Space Science and Engineering Division, Southwest Research Institute, P.O. Drawer 28510, San Antonio, TX 78228-0510, U.S.A.*
[5]*Department of Atmospheric, Oceanic, and Space Sciences, University of Michigan, 2455 Hayward Street, Ann Arbor, MI 48109-2143, U.S.A.*
[6]*Department of Physics, University of Maryland, College Park, MD, U.S.A.*
[7]*Applied Physics Laboratory, Johns Hopkins University, 11100 Johns Hopkins Road, Laurel, MD 20723-6099, U.S.A.*
[8]*Institute for Physical Science and Technology, University of Maryland, U.S.A.*
[9]*Aerospace Corporation, El Segundo, CA 90245-4691, U.S.A.*
[10]*Florida Institute of Technology, Melbourne, FL 32901, U.S.A.*
[11]*Institute for the Study of Earth, Oceans and Space, University of New Hampshire, Durham, NH 03824, U.S.A.*
[12]*California Institute of Technology, Pasadena, CA 91125, U.S.A.*

Abstract. We present ACE observations for the six-day period encompassing the Bastille Day 2000 solar activity. A high level of transient activity at 1 AU, including ICME-driven shocks, magnetic clouds, shock-accelerated energetic particle populations, and solar energetic ions and electrons, are described. We present thermal ion composition signatures for ICMEs and magnetic clouds from which we derive electron temperatures at the source of the disturbances and we describe additional enhancements in some ion species that are clearly related to the transient source. We describe shock acceleration of $0.3-2.0$ MeV nucl^{-1} protons and minor ions and the relative inability of some of the shocks to accelerate significant energetic ion populations near 1 AU. We report the characteristics of < 20 MeV nucl^{-1} solar energetic ions and < 0.32 MeV electrons and attempt to relate the release of energetic electrons to particular source regions.

1. Introduction

On 12 July 2000 (DOY 194) the Advanced Composition Explorer (ACE) spacecraft in orbit about the Earth's L1 libration point observed a strong rise in relativistic electrons in association with a chromospheric Hα flare at N17 W65 that peaked at 20:13 UT (hereafter 194/20:13 UT) (from *Solar-Geophysical Data*, see Appendix A). A commensurate rise in 1 MeV nucl^{-1} solar energetic particles (SEP)

was also observed. This was the first *in-situ* indication of what was to be a period of strong transient activity. The SEP observations, including both ions and electrons, continued for several days, with sustained levels through 16 July (DOY 198). A second Hα event peaked 196/10:21 UT at N22 W07 followed by an X5.7 X-ray flare peaking 10:43 UT (from *Solar-Geophysical Data*; Aulanier *et al.*, 2000; Kosovichev and Zharkova, 2001) which produced a second near-relativistic electron event at 1 AU. The peak of the solar activity was observed on 14 July (Bastille Day, DOY 196) from which the name of this period of activity is derived. Several interplanetary shocks were observed during these days in advance of interplanetary coronal mass ejections (ICMEs). In particular, a halo CME was observed by SOHO/LASCO on DOY 195 which resulted in an ICME observed by ACE late on DOY 197. In total, three shocks, three clouds and four ICMEs were observed by ACE in the six-day interval we study here with a fourth shock passing the spacecraft on the day before this study begins.

This wealth of activity within a short period of time offers the opportunity to study several related solar and heliospheric processes together. For instance, by studying the composition of the thermal ion charge states the electron temperature of the solar source plasma may be inferred. The inferred temperature can then be compared with the undisturbed plasma and of the ICMEs during the above solar activity. Shocks driven by the fast ICMEs accelerate the ambient thermal and suprathermal particle populations and can re-accelerate the energetic SEP population(s). The energy spectra and composition of the energetic particle populations can be examined to gain insight into the nature of the acceleration processes occurring both near the sun and within the interplanetary medium. The ACE mission is designed to facilitate precisely these comparisons (Stone *et al.*, 1998a).

We present ACE observations for the 6-day interval (DOYs 194 to 199) surrounding the Bastille Day 2000 event. We first examine the IMF, bulk plasma properties and thermal ion composition of the solar wind. With this we determine the passage of shocks, ICMEs and magnetic clouds within the 6-day period. We then examine the energetic particle populations for temporal variations in intensity, composition, and energy spectra in order to address the questions of solar injection and *in situ* acceleration processes.

2. Thermal Plasma

2.1. MAG AND SWEPAM SOLAR WIND OBSERVATIONS

The ACE spacecraft includes twin-sensor, triaxial fluxgate magnetometers (MAG) (Smith *et al.*, 1998) that provide 6 vectors s^{-1} continuously from a maximum resolution of 0.002 nT to a maximum field of 65 536 nT. The Solar Wind Electron Proton Alpha Monitor (SWEPAM) (McComas *et al.*, 1998) measures 250–35 000 eV Q^{-1} ions and 1–1370 eV electrons every 64 s. Because of high particle backgrounds, the data resolution is $\sim$ 30 min from 196/11:06 UT – 198/

01:33 UT. He^{++} measurements were unavailable from SWEPAM 196/11:00 UT – 198/01:00 UT, but are available from the SWICS instrument (see Section 2.2). Halo electron measurements are unavailable during 196/02:00 UT – 197/23:00 UT.

ICMEs are identified based on several plasma signatures, including the presence of bidirectional halo electrons (BDEs) $\gtrsim 70$ eV (Gosling, Pizzo, and Bame, 1987), high alpha/proton density ratios $\gtrsim 8\%$ (Borrini et al., 1982), and unusually low proton temperatures (Gosling, Pizzo, and Bame, 1973). A given ICME need not include all signatures (Zwickl et al., 1983) and the timing of different signatures may not be the same (e.g., Skoug et al., 2000; Burlaga et al., 2001).

Magnetic clouds, which are often coincident with ICMEs, are defined by high IMF intensity, a smooth rotation of the IMF through $\sim 180°$, and depressed proton temperatures (Burlaga et al., 1981; Lepping et al., 2001). 'Old', or evolved magnetic clouds and ICMEs are characterized by reduced velocity gradients while 'young' structures show strong velocity gradients indicative of continued expansion (Osherovich, Farrugia, and Burlaga, 1993; Osherovich and Burlaga, 1997). Old clouds generally have lower IMF intensities due to expansion.

The top four panels in Figure 1 show the interplanetary magnetic field (IMF) intensity B, latitude δ and longitude λ angles in heliographic RTN coordinates, and southward component of the IMF in GSM coordinates B_S^{GSM}. The next panels show the radial component of the solar wind velocity V_R, the proton density N_P, and temperature T_P. From these quantities, we compute the proton $\beta_P = 8\pi N_P k_B T_P / B^2$, where k_B is Boltzmann's constant, and the Alfvén speed $V_A = B/\sqrt{4\pi N_P m_P}$, where m_P is the proton mass.

The interval begins with a wind speed in excess of 500 km s^{-1} showing relatively little change over the first day. N_P and T_P are systematically and inversely variable, β_P is depressed, and the IMF direction shows a mild but persistent rotation. BDEs begin 194/$\sim$03:00 UT and continue until 195/$\sim$05:00 UT (see Table I) with elevated alpha/proton ratios (not shown) beginning 10 hr earlier. These signal the passage of an ICME (marked as ICME1 at the top of Figure 1) with an embedded magnetic cloud (Cloud1 in Table I) that is evolved and old. The cloud/ICME passes at the end of the first day and the spacecraft is once again on the open field lines (Parker, 1963). (See Table I for the timings of all ICMEs, BDEs, clouds, and shocks.)

There are then three abrupt and simultaneous rises in B, V_R, N_P, and T_P at 195/09:19:13 UT, 196/14:59:49 UT, and 197/14:16:24 UT (marked by vertical dashed lines in the figure and labeled S2, S3, and S4). Each is a forward shock, resulting in a series of step-like rises in V_R over the first four days of the interval. S4 displays only a single point of elevated N_P following passage of the shock. This is due, in part, to the reduced temporal resolution of the SWEPAM instrument at this time resulting from energetic electron contamination and is partly due to the disturbed downstream nature of the shock. Note that B, δ, and λ also show an unsteady downstream condition that prevents accurate computation of the shock normal. (See Lepping et al. (2001) for further analysis of this shock.)
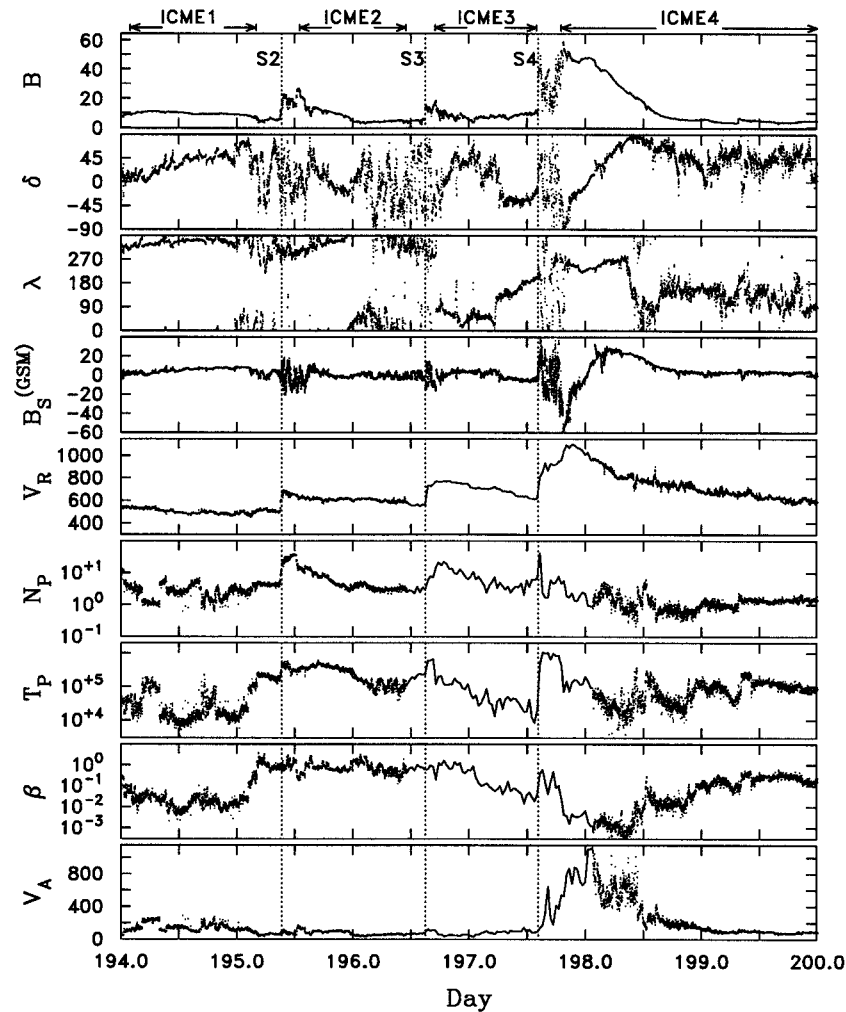
Figure 1. Overview of 6 days surrounding the Bastille Day observations. IMF intensity B (nT), latitude angle δ (deg), and longitude λ (deg) with southward component of the IMF in GSM coordinates B_S^{GSM}. Measured radial component of the wind velocity V_R (km s^{-1}), proton density N_P (cm^{-3}), and temperature T_P (K) are also shown along with computed proton β and Alfvén speed V_A (km s^{-1}). Three shocks (S2, S3, and S4) are marked by *vertical dashed lines* and 4 ICMEs are marked at top.

Each of the above shocks is driven by an ICME. ICME2 lasts from 195/ $\sim$ 13:00 UT until 196/$\sim$ 11:00 UT with both counterstreaming electrons and depressed T_P. ICME3 is difficult to resolve due to contamination by penetrating energetic electrons, but reduced T_P suggest that it lasts from 196/$\sim$ 17:00 UT until 197/ $\sim$ 14:00 UT. A second evolved cloud (Cloud3) is also present that appears to be fully expanded. The onset of ICME4 in this time period is not resolved due to the

energetic electron contamination, but it appears to begin 197/$\sim$ 19:00 UT and lasts until 200/$\sim$ 12:00 UT. The elevated alpha/proton ratios end somewhat earlier.

The exceptionally high B period following S4 also shows a smooth, systematic rotation of the IMF direction and reduced β_P signalling a third magnetic cloud (Cloud4). The high B and strong V_R gradient indicate that this is a young and relatively unevolved structure that is still expanding. Although V_A is fairly typical over much of the six-day interval, and only somewhat elevated during some periods in the first few days, a greatly enhanced V_A is observed in association with the magnetic cloud late on day 197 and into day 198. The expansion of the object has resulted in nearly sub-Alfvénic flow during this time.

At the same time that B reaches large values late on day 197, the field turns southward. B_S^{GSM} briefly surpasses -59 nT and for a prolonged period surpasses -30 nT. At the same time, $V_R > 1100$ km s^{-1}. Thus, an exceptionally strong southward IMF is impacting the Earth's magnetosphere with exceptional speed, providing a configuration that is highly conducive to magnetic reconnection at the Earth's magnetopause and associated storm activity (Mitchell *et al.*, 2001; Jordanova *et al.*, 2001). Following this, V_R tapers off over several days, the IMF is steady in magnitude and direction, and N_P and T_P are essentially constant. Additional shocks are seen in the few days following and before this period.

Putting together the ICME and cloud times, it is clear this 6-day period is composed almost entirely of a series of solar ejecta with relatively little time between transients. All but one of these ICMEs contain a magnetic cloud. Each drives an interplanetary shock. We will number the four disturbances 1–4 and from here on use this notation to refer to the shocks, ICMEs, etc. Table I lists each disturbance and their associated times.

2.2. SWICS THERMAL ION COMPOSITION OBSERVATIONS

The Solar Wind Ion Composition Spectrometer (SWICS) is a combination of an electrostatic analyzer, a linear time of flight, and a solid state detector system with post acceleration (Gloeckler *et al.*, 1998). Using triple coincidence, the combination of detector subsystems determines unambiguously the mass, charge, and speed of most detected ions with 12 m resolution.

0 Figure 2 (left) shows the elemental composition of solar wind ions during days 195–198. We show, from top to bottom, elemental ratios He/H, He/O and Fe/O. Vertical dashed lines indicate the locations of shocks S2, S3, and S4 (see Table I) and ICMEs are marked at the top of the figure. Each compositional parameter varies considerably during this interval. ICME2 is similar to an average slow solar wind composition of H/O $= 1900 \pm 600$, He/O $= 80 \pm 30$, and Fe/O $= 0.12 - 0.19$ (von Steiger, Geiss, and Gloeckler, 1997). The variations observed during this period are typical of the average compositional variations within slow solar wind (e.g., Zurbuchen *et al.*, 2000). In contrast, ICME3 and ICME4 show clear deviations from the slow solar wind composition. First, He is enhanced during ICME3

TABLE I

Transient times.

Type	Time (DOY/time (UT))[a]	
Shock1	193/11:23:06[b]	
Cloud1	194/00:00 (start)	195/00:00 (end)
ICME1	194/02:00 (start)	195/04:00 (end)
BDE1	194/03:00 (start)	195/04:00 (end)
Shock2	195/09:19:13	
ICME2	195/13:00 (start)	196/11:00 (end)
BDE2	195/13:00 (start)	unresolved[c] (end)
Shock3	196/14:59:49	
ICME3	196/17:00 (start)	197/14:00 (end)
Cloud3	197/06:00 (start)	197/14:00 (end)
Shock4	197/14:16:24	
Cloud4	197/19:00 (start)	198/10:00 (end)
ICME4	197/19:00 (start)	200/12:00 (end)
BDE4	unresolved[c] (start)	200/12:00 (end)

[a]Start and end times of clouds and ICMEs are approximate.
[b]Shock occurs within previous 8 s.
[c]BDE start/end times unresolved due to energetic electron contamination.

as reflected in enhanced He/O and He/H ratios. The FIP fractionation, measured by Fe/O, is nominal and similar to the first event. ICME4 again shows enhancements in He/H and He/O. However, Fe/O is clearly depleted compared to average solar wind values. Note also that the composition is not constant during this event. For example, the Fe/O ratio increases by almost one order of magnitude from ~ 0.02 to ~ 0.1.

Figure 2 (right) shows the ionic composition of the ICME events. We show $T(O^{7+}/O^{6+})$, the local thermal equilibrium freeze-in temperature calculated from the O^{7+}/O^{6+} ratio. We also show C^{6+}/C^{5+} and the average Fe charge state. ICME2 has charge state signatures typical of the slow solar wind. ICME3 exhibits a non-uniform temperature distribution for all ionic charge distributions shown in Figure 2. The charge state distributions suggest electron temperatures in the corona that are close to 3 MK. Similar temperatures are also found in ICME4. There are subtle differences between the events, presumably relating to different temperature histories of the two ejecta.

These hot charge distributions are found in approximately half of all ICMEs as identified by plasma signatures and bidirectional electron events (Lepri *et al.*, 2001). Magnetic clouds are more likely to be associated with such hot charge state
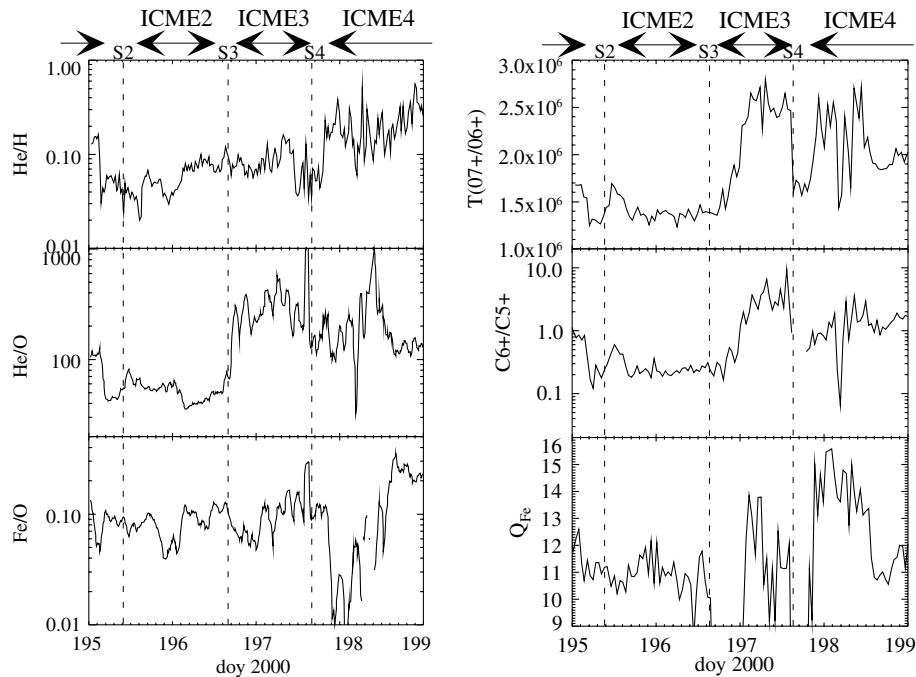
Figure 2. Left: thermal ion composition ratios measured by the SWICS instrument. ICMEs and shocks are marked at top. *Right*: source region electron temperature inferred from oxygen charge state ratios, carbon charge state ratios, and average iron charge state as obtained by the SWICS instrument.

distributions (Henke *et al.*, 1998). This was also reported by Burlaga *et al.* (2001) who found O^{7+}/O^{6+} enhancements for all magnetic clouds in their study. The time period with the unusual composition signatures did not always fill the entire ICME period, as determined using bidirectional electron signatures. Our results are in good agreement with these studies. The C^{6+}/C^{5+} ratio also freezes in the low corona, similar to O^{7+}/O^{6+}. It is therefore not surprising that there is a great deal of similarity between the curves in the first 2 panels of Figure 2 (right). Typically, the C freeze-in temperature is lower than for O by $\sim 25\%$ (von Steiger, Geiss, and Gloeckler, 1997). ICME2 has typical slow solar wind composition, whereas ICME3 and ICME4 have unusual signatures consistent with magnetic clouds. Note that ICME3 and ICME4 are separated by a period of slow solar wind composition.

   Elemental and charge state signatures indicate that the physical environment where ICME2 originated is clearly different from the likely origin of the last two events. The lack of unusual compositional signatures during ICME2 shows its common source with average slow solar wind (Zurbuchen *et al.*, 2000). Both of the latter events have an enhanced He/H and ICME4 has a clearly depleted Fe/O abundance. These signatures are not consistent with average solar wind composition. They reflect unusual, possibly time-dependent coronal conditions. The unusual

TABLE II

EPAM electron data[a]

Electrons (MeV)	2000 Backgrounds $(cm^2 \, sr \, s \, MeV)^{-1}$	N17 W65 194/20:13 UT $(cm^2 \, sr \, s \, MeV)^{-1}$		N22 W07 196/10:21 UT $(cm^2 \, sr \, s \, MeV)^{-1}$	
		pre-event	peak	pre-event	peak
DE1 0.39c (0.038–0.053)	1.51×10^2	5.87×10^3	6.65×10^4	3.62×10^4	1.09×10^7
DE2 0.49c (0.053–0.102)	6.70×10^1	1.33×10^4	1.21×10^4	7.04×10^3	4.13×10^6
DE3 0.61c (0.103–0.175)	3.31×10^1	5.49×10^2	2.83×10^3	2.03×10^3	2.18×10^6
DE4 0.71c (0.175–0.315)	1.27×10^1	1.24×10^2	4.44×10^2	3.81×10^2	7.54×10^5

[a]EPAM electron intensities (Figure 3, panel A).

ionic composition is indicative of a large heating and subsequent fast expansion of the CME-associated plasma. The freeze-in temperatures of ~ 3 MK should be considered a lower limit for the maximum electron temperature during the CME expansion.

3. Energetic Particles

ACE observed energetic particle populations both accelerated near the sun and those energized nearer 1 AU. We begin with the electrons and lower energy ions.

3.1. EPAM ENERGETIC ELECTRON AND ION OBSERVATIONS

The Electron, Proton, and Alpha Monitor (EPAM) measures ion and electron intensities (Gold *et al.*, 1998). The deflected electron detector (DE) measures electron intensity in four logarithmically spaced channels from 38–315 keV. The composition aperture (CA) determines ion composition from 0.047–5.0 MeV using a $\Delta E \times E$ detection scheme.

Near-relativistic electrons: Two major increases are observed in the near-relativistic electrons (Figure 3, panel A). The onset of the first electron event at 194/20:25 UT is demarcated by intense beams of electrons flowing along the IMF (distribution not shown). Correlation with solar radio observations indicates that this event is associated with a chromospheric Hα flare (N17 W65) that peaked at 20:13 UT with 15 400 MHz and 8800 MHz radio bursts peaking at 20:10 UT and a type II/2 coronal shock that was first identified at 20:14 UT (see Appendix A). The
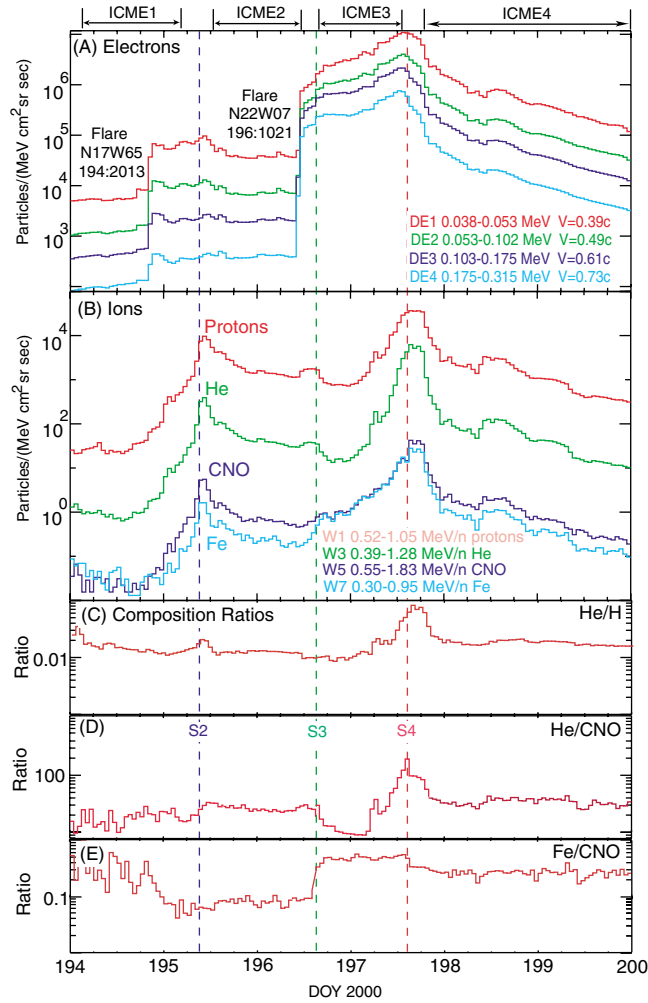
Figure 3. (A) shows near-relativistic electron intensities (Table II). (B) shows ion intensities for protons, alphas, CNO, and iron (Table III). The He/H, He/CNO, and Fe/CNO composition ratios are shown in (C), (D), and (E) respectively. The alpha and iron composition channels contain particles of a few hundred keV lower then the protons and CNO composition channels. The *red traces* in panels C-E have been modified by the species specific energy spectra obtained by the ULEIS instrument and for the narrow energy range applicable here are of the form $dJ/dE = Ae^{-\gamma}$ where γ is the power-law spectral exponent. The curves prior to S3 were obtained using $\gamma = 2$ while the curves after S3 used $\gamma = 1$.

second and much more intense electron onset at 196/10:39 UT represents the initial *in-situ* observations of electrons arriving from the massive Bastille Day event. The DE4 electron intensity (Table II) rapidly rose from a pre-event level of 3×10^2 to a level of 1×10^5 particles $MeV^{-1} cm^{-2} sr^{-1} s^{-1}$ in one hour, then required an additional 26 hours to increase by a factor of six. The solar electromagnetic signatures

TABLE III

EPAM ion composition data[a]

Species (MeV nucl^{-1})	2000 Backgrounds (cm^2 sr s MeV)$^{-1}$	July 13 195/09:18 UT (cm^2 sr s MeV)$^{-1}$		Bastille Day shock 197/14:15 UT (cm^2 sr s MeV)$^{-1}$	
		pre-event	peak	pre-event	peak
Protons (0.52–1.05)	9.74×10^{-1}	2.54×10^{1}	9.66×10^{3}	7.81×10^{2}	3.70×10^{4}
Helium (0.39–1.28)	1.64×10^{-3}	1.27×10^{0}	3.73×10^{2}	1.33×10^{1}	5.99×10^{3}
CNO (0.55–1.83)	3.62×10^{-4}	3.64×10^{-2}	5.57×10^{0}	5.84×10^{-1}	3.92×10^{1}
Iron (0.30–0.95)	1.86×10^{-4}	3.64×10^{-2}	1.65×10^{0}	2.06×10^{-1}	2.65×10^{1}

[a]EPAM ion intensities (Figure 3, panel B).

of the Bastille Day event include an X5.7 X-ray event, 15 400 MHz radio bursts, a coronal type II/3 shock and a flare located at N22 W07. During the onset of the Bastille Day event, the Earth was not well connected to N22 W07 (the presumed center of the coronal shock) along the IMF spiral. A series of interplanetary shocks and disturbances preceded the arrival of the Bastille Day event; thus we attribute the 26-hr slowly rising electron intensity increases to a combination of spatial effects. First is the convection of field lines that connect the spacecraft to different points along the approaching CME-driven shock. Temporal and dynamical effects due to scattering and magnetic reflection (mirroring), and resultant partial confinement of electrons to the inner heliosphere by the disturbed IMF regions beyond 1 AU also affect the electron intensities.

Ion composition: The ion composition channels (Figure 3, panel B) contain somewhat different energy ranges yet can be categorically described as 0.5– 1.0 MeV nucl^{-1}. The ions shown are protons, helium, carbon-nitrogen-oxygen (CNO), and iron. The two main intensity peaks correspond well with the two interplanetary shocks S2 and S4 (Table I). Prior to day 194 the ion and electron intensities in the inner heliosphere were already significantly enhanced over background due to energetic particle injections by dynamic solar activity and by a series of interplanetary shocks.

The first indication of the approaching interplanetary shock (S2) was an increase in the ion intensities that began at 194/20:04 UT. The intensities of all ion species began to rise until the shock's arrival. The duration of time that the shock influenced the energetic particle intensities at 1 AU was $\sim$ 13 hr. Although the intensity increases of the shock-accelerated energetic particles are somewhat masked by the

already high pre-event levels, the increases are at least two orders of magnitude for H, He, and CNO, and a factor of 45 for Fe (Table III).

The duration of the S4 shock-accelerated population is obscured due to two related factors. One is the presence of the smaller shock S3 while the other is an unusual 13-hr decrease in the intensity of H and He ions immediately after the S3 shock. A clear increase in the H and He intensities associated with the approaching S4 shock was observed at 197/04:57 UT and continued for over nine hours until the arrival of S4. The CNO and Fe intensities, which did not show the 13-hr decrease seen in H and He, started to rise at S3, and continued to increase for over 20 hours until the arrival of S4. The ion intensities were already significantly enhanced at the time the effects from S4 were first observed, yet showed additional intensity increases (factor of 47 for H, 452 for He, 67 for CNO, and 128 for Fe).

Composition ratios: Ion composition ratios are known to vary within events and from event to event. Panel C of Figure 3 shows the He/H ratio. Panel D shows the He/CNO ratio and Panel E shows the Fe/CNO ratio. The composition ratios shown in Figure 3 have been modified according to the energy spectra observed by the ULEIS instrument (see Figure 5) to account for the differing passbands of the composition channels. Spectra are unavailable during the time periods shown in Figure 4, therefore during these periods the composition ratios in Figure 3 reflect ratios based on spectra measured prior to and after the indicated periods.

Composition ratios associated with S2 show no significant shock-associated variations other than a small increase in the He/H ratio near the shock. This is in stark contrast to the widely varying ratios observed between the S3 and S4 shocks. Because the dramatic intensity drop after S3 is observed in both the H and He ions, the He/H ratio remains nearly constant (~ 0.02), similar to the levels reported by Mazur *et al.* (1993), until a strong helium increase at 197/04:57 UT. The He/H ratio then increases with the approaching shock to a peak ratio of 0.09.

As already noted, the intensity drops in H and He after S3 are not observed in CNO or Fe. This produces the strong drop in the He/CNO ratio after S3 (panel D). Prior to S3, the He/CNO ratio is ~ 30, only slightly below the level found by Mazur *et al.* (1993). After S3, the ratio drops below 10 and remains low until 197/04:57 UT. It then increases to over 200 at S4 before declining to a nominal value of ~ 40 over the next ~ 8 hours.

The Fe/CNO ratio (panel E) is variable and slightly lower compared to levels found by Mazur *et al.* (1993). However, after S3 the Fe/CNO ratio rises to 0.6, a level somewhat below the level found in in smaller [3]He rich events and in an occasional well-connected western events (Reames, 1990). The ratio remains ~ 0.6 until after S4 when it returns to typical levels (Mazur *et al.*, 1993).

3.2. ULEIS ENERGETIC ION COMPOSITION OBSERVATIONS

The Ultra Low-Energy Isotope Spectrometer (ULEIS, Mason *et al.*, 1998) is a high-resolution mass spectrometer that identifies nuclei from H through Fe in the
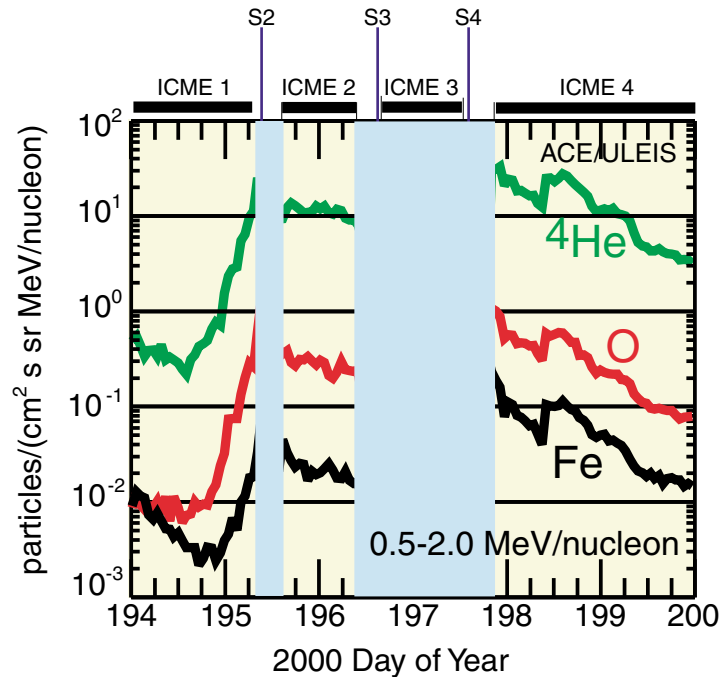
Figure 4. (a) Intensity–time profiles of 0.5–2.0 MeV nucl^{-1} ^{4}He, O, and Fe nuclei measured by ULEIS. The 3 interplanetary shocks observed at ACE during this period are identified at the top along with the 4 ICMEs. *Blue regions* identify time periods during which the instrument saturated as a result of intense particle fluxes, while *yellow regions* identify time intervals during which the response of ULEIS was nominal. ICME2 and ICME4 are selected for further analysis.

energy range 0.02–10 MeV nucl^{-1} by performing time-of-flight vs. residual energy measurements for each ion.

Figure 4 shows the intensity of 0.5 to 2.0 MeV nucl^{-1} ^{4}He, O, and Fe. Due to the high level of particle flux, ULEIS saturated around the passage of all three interplanetary shocks (S2, S3, and S4; blue regions obscure these periods). EPAM measurements (Figure 3) indicate that S3 did not accelerate a significant number of particles locally. We therefore focus our analysis toward understanding the origin and acceleration of energetic particles at S2 and S4 and select ICME2 and ICME4 for further analysis. These periods satisfy the following criteria: (1) The intensities of all species track each other within a factor of 2, and (2) The periods correspond to spatial regions downstream of the shocks.

The upper panels in Figure 5 show energy spectra of various ion species measured by ULEIS and SIS (see Section 3.4) spanning 0.02–200 MeV nucl^{-1}. The differential energy spectra of various species (upper panels of Figure 5) show several differences downstream of S2 and S4. The intensities of all species below ~ 0.5 MeV nucl^{-1} are about an order of magnitude greater within ICME2 (donwstream of S2) than within ICME4 (downstream of S4). The opposite effect
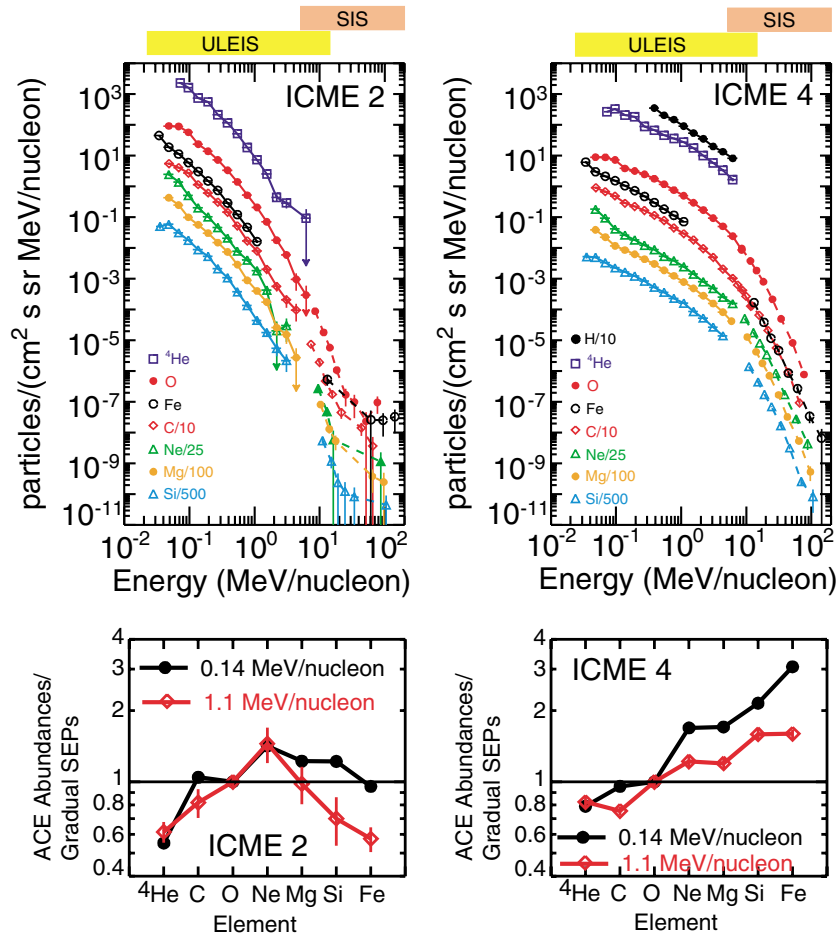
Figure 5. Upper panels: Energy spectra of various ion species measured by ULEIS and SIS (see Section 3.4) during the Bastille Day event. Energy ranges of each instrument are marked at top. *Lower panels*: heavy ion abundances compared with 4–5 MeV nucl^{-1} abundances measured in gradual SEPs (from Reames, 1999). All abundances are normalized to O. ULEIS abundances are shown at ~ 0.14 MeV nucl^{-1} and ~ 1.1 MeV nucl^{-1}. The *left* and *right panels* show data from ICME2 and ICME3.

is observed for ions above 0.5 MeV nucl^{-1}, indicating that the energy spectra of all species in ICME2 are softer than those in ICME4. The spectra measured by ULEIS during both ICMEs can be adequately represented by a power law times an exponential in energy (e.g., Tylka *et al.*, 2001). From fitting these functional forms to the energy spectra for all species we have determined that the average values for the spectral index γ and the *e*-folding energy E_0 during ICME2 were ~ 1.8 and ~ 0.8 MeV nucl^{-1} while during ICME4 they were ~ 1.0 and ~ 3.5 MeV nucl^{-1}, respectively.

The lower panels of Figure 5 show the oxygen-normalized heavy ion abundances between $0.11-0.16$ MeV $nucl^{-1}$ and $0.91-1.28$ MeV $nucl^{-1}$ (~ 0.14 and ~ 1.1 MeV $nucl^{-1}$, respectively) during ICME2 and ICME4. The ULEIS abundances are further normalized to $4-5$ MeV $nucl^{-1}$ abundances averaged over several large gradual SEP events (Reames, 1999). With the notable exception of ^{4}He, the heavy ion abundances during ICME2 at ~ 0.14 MeV $nucl^{-1}$ are close to unity and exhibit no significant enhancements over average gradual SEP abundances. The abundances of ^{4}He and Fe at ~ 1.1 MeV $nucl^{-1}$ during ICME2 are a factor of ~ 2 lower than those measured in gradual SEP events. The abundances of C and Si exhibit similar behavior, but with larger uncertainties. The ion enhancements at both energies during ICME2 show no systematic trend with mass, whereas those measured during ICME4 show a systematic increase with mass. The C, Ne, Mg, Si, and Fe enhancements at ~ 1.1 MeV $nucl^{-1}$ during ICME4 are a factor of ~ 2 lower than at ~ 0.14 MeV $nucl^{-1}$.

It is interesting to note that Desai *et al.* (2001) found that the ^{3}He/^{4}He ratios at $0.5-2.0$ MeV $nucl^{-1}$ associated with S1 and S2 were 0.043 ± 0.037 and 0.0023 ± 0.0008, respectively, indicating that the ^{3}He abundance was enhanced above the slow solar wind value of 4×10^{-4} (Gloeckler and Geiss, 1998). These results were interpreted as consistent with a scenario in which the interplanetary shocks accelerate ions from multiple sources, one being remnant impulsive SEP material enriched in ^{3}He ions, as suggested by Mason *et al.* (1999). The presence of highly ionizied Fe during these events as measured by SEPICA (see Figure 6) provides additional comfirmation that remnant impulsive SEP material is reaccelerated at these two shocks.

The fact that the energy spectra can be represented by a power law times an exponential has typically been attributed to a charge/mass (Q/A) or rigidity dependent acceleration or leakage process (e.g., Tylka *et al.*, 2001). In this process particles of lower rigidity are scattered more easily and accelerated more efficiently at the shock (Lee, 1983), and conversely particles of higher rigidity escape more easily from the acceleration region. According to this model one expects the ion enhancements to decrease for the heavier or higher rigidity ions near the shock (Klecker *et al.*, 2000) while the opposite effect should occur away from the shock. We find that at the same energy per nucleon the heavier ion abundances during both periods are enhanced when compared with lighter ions. In fact, the ion abundances in ICME4 show a systematic increase with increasing mass or rigidity. This feature was first reported by Breneman and Stone (1985) and observed by Mason *et al.* (1999) during the November 1997 SEP event. We suggest that the heavy ion enhancements during ICME2 and ICME4 cannot be explained if the ion populations are dominated by acceleration effects, but could possibly be explained if ion transport effects dominate the observations.

ICME2 and ICME4 are different from the November 1997 event in that the heavy ion abundances at ~ 1.1 MeV $nucl^{-1}$ are a factor of 2 lower than those observed at ~ 0.14 MeV $nucl^{-1}$. This trend continues for Fe and Ne (but not C) at 12

-60 MeV nucl^{-1} as observed by the SIS instrument (see Figure 5 and Section 3.4). In contrast, during the November 1997 event there were no significant differences in the heavy ion abundances at ~ 0.15 MeV nucl^{-1} and 1.5 MeV nucl^{-1}, while the $12-60$ MeV nucl^{-1} abundances measured by SIS were substantially enhanced. While the energy-dependent elemental enhancements shown here could be due to the presence of higher charge state Fe at higher energy (SEPICA is unable to confirm this possibility at this time), this explanation cannot account for the November 1997 observations which did have higher ionization states at higher energies (Möbius *et al.*, 1999). Finally, the ULEIS and SIS spectra in Figure 5 indicate that the intensity of energetic particles $\lesssim 0.5$ MeV nucl^{-1} associated with S2 is significantly greater than for S4, whereas S4 possesses a greater intensity of $\gtrsim 0.5$ MeV nucl^{-1} particles. Clearly S4 poses a more severe radiation hazard to astronauts (e.g., Reames *et al.*, 2001).

3.3. SEPICA ENERGETIC ION COMPOSITION OBSERVATIONS

The Solar Energetic Particle Ionic Charge Analyzer (SEPICA) instrument measures element fluxes and ionic charge states of ions from H through Fe (Möbius *et al.*, 1998). The energy range for element fluxes is $0.2-5$ MeV nucl^{-1}, and for charge states is $0.5-3$ MeV Q^{-1}. The instrument is an energy loss/residual energy telescope, utilizing a 30 kV deflection voltage for charge state measurements.

Data from SEPICA are shown in Figure 6. From top to bottom are: the O flux at 0.54 MeV nucl^{-1}, the H flux at 0.75 MeV nucl^{-1}, the Fe/O ratio at 0.54 MeV nucl^{-1}, charge states for individual Fe ions and the average Fe charge state for 8 hour intervals. The average energy for Fe charge state measurements is 0.25 MeV nucl^{-1}. Shocks are indicated by vertical dashed lines (S1–S4). Cloud1 is marked 'cloud candidate' because an earlier start time is used due to the continuous arrival of high charge state Fe ions.

Fe charge states for most of this period were ~ 10, typical of an ICME-driven interplanetary shock event. A period of unusual charge states was observed from 193.75 to 195.1 (Figure 6) to be approximately coincident with Cloud1 (vertical dash-dot lines). This interval is a superset of the cloud interval identified by MAG and SWEPAM. During this time, the average Fe charge state was as high as 15, and the Fe/O ratio was ~ 1. These are typical signatures of flare-related impulsive events. X-ray flares occurred during this time from AR 9070 at western solar longitudes and AR 9077 at eastern solar longitudes (see Appendix A). Immediately after the cloud passage, the Fe/O ratio and Fe charge state declined to approximately 0.1 and 10+, and remained that way until the passage of S3. The end of Cloud1 is defined by the magnetic field rotation (Table I), but the charge state composition changed somewhat before that. H and O fluxes also began to increase somewhat before the end of the rotation.

All ion fluxes responded to S2. In contrast, S3 showed little response in heavy ions. Only H showed a flux increase. The 30 kV deflection high voltage dropped
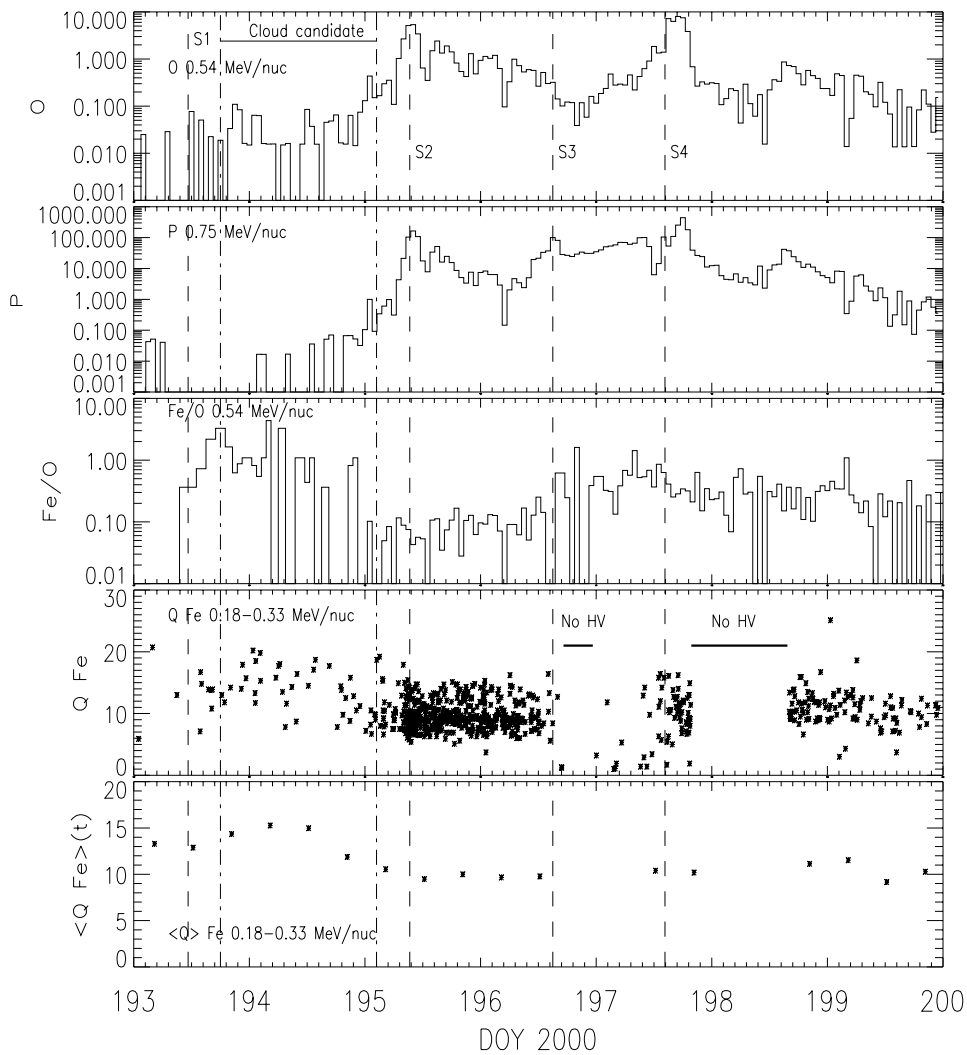
Figure 6. SEPICA observations (*top to bottom*): 0.54 MeV nucl^{-1} O flux and 0.75 MeV nucl^{-1} H flux [particles cm^{-2} sr-1 s^{-1} MeV^{-1} nucl], Fe/O ratio at 0.54 MeV nucl^{-1}, charge states for individual Fe ions, and the average Fe charge state for 8 hours. *Vertical dashed lines* show Cloud1 and 4 shocks (S1–S4).

at 196/17:00 UT and recovered partially at 197/00:00 UT. During this time, heavy ion fluxes could be measured, but no charge states could be calculated. Between 197/00:00 UT and 197/19:45 UT, the mean charge state of Fe remained at ∼ 10. Charge states near zero or one at this time are not credible because of the moderate deflection voltage. This period includes the most intense fluxes from ∼ 14:20–19:10 UT. During the highest fluxes, the lifetime decreased to zero, but individual charge state measurements could still be made. The quantity of Fe collected at this

time was low because the instrument was triggering instead on very low energy protons, with signals just above threshold. In addition, the anticoincidence detector rate, which is sensitive to penetrating ion fluxes, rose substantially during this time. Although the fluxes have been corrected for lifetime, only a partial correction can be made when the lifetime goes to zero. Therefore, the calculated fluxes during the 14:20−19:10 UT period represent lower limit estimates of the actual fluxes.

The high voltage again dropped 197/19:30 UT to 198/16:30 UT. Two magnetic clouds (Cloud3 and Cloud4) passed the spacecraft during this time. A clear decrease in heavy ion fluxes occurred during cloud passage and the Fe/O ratio was variable between 0.09 and 0.9. From the recovery of the high voltage until another ICME/cloud beginning $\sim$ 202/00:00 UT (not shown), the Fe/O ratio was variable between 0.07 and 1.0. Most of the Fe had a charge state $\sim$ 10, with some occasionally as high as $\sim$ 20. During this time, AR 9077 was moving off toward western longitudes, where magnetic connection between the active region and the Earth should be favorable for direct observation of impulsive, flare-related events. During the field rotation, the charge state 10 component weakened substantially and higher charge state Fe was introduced. The higher charge Fe continued until 203/$\sim$ 20:00 UT.

Apart from the magnetic cloud periods, the Fe charge state throughout the Bastille Day activity is typical of what is seen in CME-driven interplanetary shock events. It is interesting, however, to compare the period before the flux maximum to the period afterward. In both periods, there were X-ray flares from active regions at western longitudes (Appendix A). It is reasonable therefore to expect the SEPs in both periods to be from a mixture of impulsive and gradual sources. In the period before the flux maximum, 195/03:00 UT to 196/14:00 UT, the Fe/O ratio at 0.54 MeV nucl^{-1} was consistently low, and the mean Fe charge state was 10. In the period following Bastille Day, however, from 198/14:00 UT to 202/00:00 UT (not shown), there was a moderate component of high charge state Fe. The Fe/O ratio was higher in this later period and variable, although generally <1. Elevated Fe/O ratios are associated with impulsive events, and the admixture of a minor component of impulsive SEPs might create the variability in the Fe/O ratio observed after the flux maximum. Indeed, some high charge state Fe ions were observed in the post-maximum period from 198/14:00 UT to DOY 202. The lack of an impulsive component in the pre-maximum period from 195/03:00 UT (before ICME2) through Cloud4 might be caused by the substantial distortion in the IMF associated with the presence of multiple magnetic clouds including Cloud4 and the cloud in transit which is subsequently observed on DOY 202. If true, access to the Earth from the western solar longitudes was poor at this time.

Cloud1 contained significantly more high charge state Fe than any other period, including the gradual/impulsive mixture after Bastille Day. In addition, the Fe/O ratio for Cloud1 was high, at $\sim$ 1. These signatures suggest that SEPs in Cloud1 originated in an active region. They may have been shock accelerated out of the solar wind or out of the suprathermal flare population previously existing within

the cloud. The shock S2 that passed the spacecraft after Cloud1 could have reac-
celerated these ions. Alternatively, they may have originated in a more recent flare
at the footpoint of the cloud, but the absence of velocity dispersion in the ULEIS
data (not shown) suggests shock interaction with the flare ions or multiple flare
sources. The source region for Cloud1 might be AR 9077 or possibly 9070. During
passage of the day 202 magnetic cloud, there were no X-ray flares at western solar
longitudes. The source region for this cloud might then be an active region on the
disk.

3.4. SIS ENERGETIC ION COMPOSITION OBSERVATIONS

The Solar Isotope Spectrometer (SIS) measures energetic ions from ~ 5 to
200 MeV nucl^{-1} and consists of two telescopes with a combined geometry fac-
tor of ~ 40 cm^2 sr (Stone *et al.*, 1998). Using the dE/dx versus residual energy
technique, the nuclear charge, mass and total kinetic energy can be determined for
incoming particles. Mass resolution of ~ 0.15 to > 0.3 amu is obtained, depending
on E and Z.

From these data, elemental intensities, spectra and abundance ratios can be de-
termined and are shown in Figure 7 for DOYs 194–200 of 2000. The intensities
of 7–13 MeV nucl^{-1} O, 9–17 MeV nucl^{-1} Si, and 10.5–21.5 MeV nucl^{-1} Fe are
given in the top panel. The small event on DOY 195 is apparent in the O intensities,
but was not large enough to result in a significant increase in Fe at these energies.
The large SEP event on DOY 196 starts shortly before noon and lasts for many
days, peaking around 197/12:00 UT. The intensities smoothly decay over a period
of several days, with a depression in the intensities of all species during Cloud4
(indicated by the yellow bar). Such a feature is seen at lower energies by EPAM,
ULEIS, and SEPICA sensors (Figures 3, 4, and 6). S3 and S4 appear to have little
effect on the particle intensities at these energies, in contrast to observations at
lower energies which show strong intensity enhancements at S4.

Daily averaged spectra for O, Si and Fe are presented in the middle panel of
Figure 7. On DOYs 194 and 195 (and on DOY 199 for Fe) contributions from
galactic cosmic rays are evident in the spectra at energies above ~ 50 MeV nucl^{-1}.
The small event on DOY 195 can be seen in the spectra with increases at the lower
energy ranges by a factor of ~ 5 to 10. On DOY 196 the Bastille Day event pro-
duces particle intensities 3 to 4 orders of magnitude greater than on DOY 194, with
solar particles accelerated well above 100 MeV nucl^{-1}. The ULEIS observations
suggest that at SIS energies the spectra should be exponential in shape. This is true
for O for DOY 196, but not for DOY 195 which is better described by a power law
in energy. However, the Si and Fe spectra are not quite exponential, as the higher
energy intensities do not decrease as rapidly as would be expected. This can also
be seen in Figure 5 (upper panels) where the combined ULEIS and SIS spectra for
ICME2 and ICME4 are given. In ICME4 there is a clear hardening of the spectra
above ~ 20 MeV nucl^{-1}. The possible similar behavior in ICME2 is obscured by
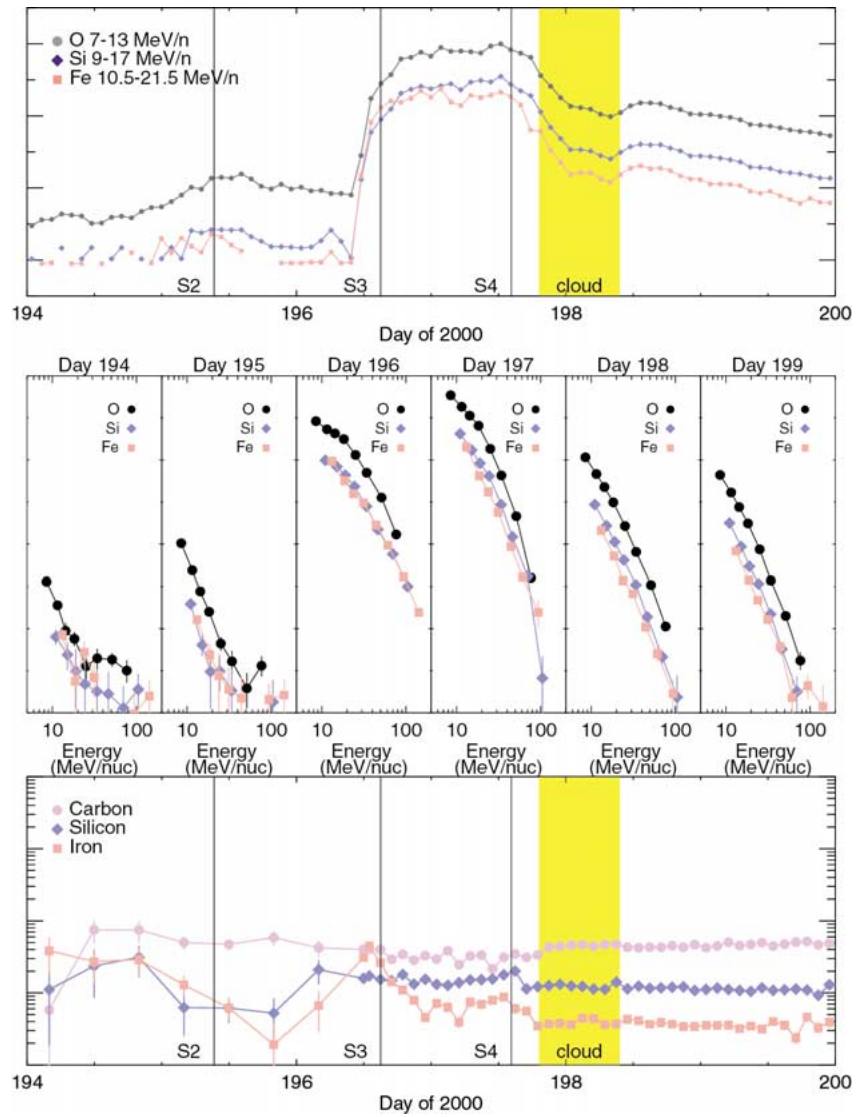
Figure 7. SIS intensity time profiles for O, Si, and Fe (*top panel*); daily averaged elemental spectra for O, Si and Fe (*middle panel*); and abundances relative to O over 12 to 60 MeV nucl^{-1} for C, Si, and Fe using 8-h and 2-h averages (*bottom panel*). Typical gradual SEP abundances for these elements are given along the right-hand side of the plot. In the top and bottom panels, *vertical lines* denote identified shocks and a *yellow shaded region* indicates the passage of Cloud4.
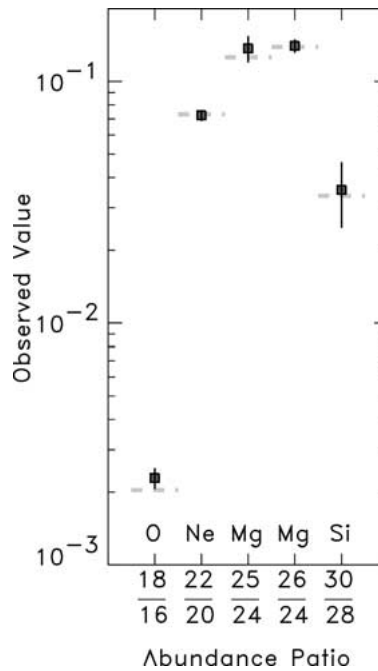
Figure 8. Isotope abundance ratios measured by SIS during the Bastille Day event. *Horizontal dash-dotted lines* mark the solar system values of Anders and Grevesse (1989).

the presence of galactic cosmic rays above 20 MeV nucl^{-1}. This nonexponential behavior could be a result of the different Q/A ratios of the elements. Tylka *et al.* (2000) successfully fit spectra of H to Fe over an energy range from a few to several hundred MeV nucl^{-1} using a spectral form that is a power law modulated by an exponential. In this model the *e*-folding energy is proportional to a power of Q/A for each species. By adding a 5% contribution of higher-charge state material (mostly affecting the Fe distribution), Tylka *et al.* (2001) were able to reproduce such spectral hardening at higher energies. Such an admixture can also explain observations of energy dependent charge states, a feature that was seen in the 6 November 1997 event (Möbius *et al.*, 1999; Mazur *et al.*, 1999). However, for reasonable assumptions of the Q/A values, one would not be able to reproduce the suggested cross-over of the O and Fe spectra above 70 MeV nucl^{-1} that is seen in the DOY 197 spectra in the second panel of Figure 7. Such a feature is most likely related to time dependent effects.

Abundance ratios relative to O are calculated by integrating the spectra over 12−60 MeV nucl^{-1} and are presented in the bottom panel of Figure 7 for C, Si, and Fe. Prior to the Bastille Day event, 8-hr averages are used to improve statistical accuracy; after 196/12:00 UT, 2-hr averages are used. For reference the abundance ratios of typical large gradual SEP events (Reames, 1999) are given just outside the right y-axis. The C/O and Si/O ratios when integrated over ICME4 are nominal,

while the Fe/O ratio is depressed by a factor of ~ 3. In contrast, the ULEIS Fe abundances at 0.14 MeV nucl^{-1} are enhanced by a factor of ~ 3 when compared with large gradual SEP events (see Figure 5).

At the start of the Bastille Day event there is a significant increase in the Fe/O ratio (by about 3 times the typical value) which then decreases over a period of 12 hours. Additionally there is a slight change in all the abundance ratios when S4 passes the spacecraft, which could also be related to properties of Cloud4. Similar features are apparent in the EPAM data, however the Fe/O values at S3 are higher and remain elevated until the passage of S4. It is apparent in the energetic particle observations at all energies (Sections 3.1–3.4) that while the intensities are slightly suppressed during Cloud4, recovering to higher values as the spacecraft exits the cloud, this is not true for the abundance ratios. Although the ratios decrease just prior to the start of Cloud4, there is no change upon exit. In fact, the abundance ratios are remarkably constant throughout DOYs 198 and 199. Similar signatures at the start of the event are seen at lower energies by the LEMT instrument on WIND (Reames *et al.*, 2001). However, the LEMT composition signatures show more variation during the passage of Cloud4.

A sample of SEP isotope measurements during the Bastille Day event is shown in Figure 8. These measurements were made with SIS at an energy which depends somewhat on the species but was ~ 15 to 70 MeV nucl^{-1} for Ne. Because of the soft energy spectrum and limited counting statistics at these energies, we have only determined the isotopic composition integrated over the duration of the event. During the very high rate periods at the peak of the event, resolution was degraded due to chance coincidences with other particles, so this plot includes data from DOYs 198–200, after the highest intensities had subsided. The isotopic composition is remarkably similar to that of the standard 'solar' abundance compilation of Anders and Grevesse (1989), indicated by the dashed lines, for isotope ratios varying by nearly two orders of magnitude in abundance ^{18}O/^{16}O to ^{26}Mg/^{24}Mg. This is quite unlike some other large SEP events observed by SIS, in which the ^{22}Ne/^{20}Ne ratio, for example, was sometimes enhanced by a factor of ~ 3 (Leske *et al.*, 1999). Thus, in both their elemental and isotopic composition, the > 10 MeV nucl^{-1} SEPs observed in the Bastille Day event appear nearly unfractionated.

4. Summary

We have examined a 6-day period (2000, DOYs 194–199) of ACE measurements at 1 AU focussing on the Bastille Day transients and their associated energetic particle populations. We have identified a series of shocks, ICMEs and magnetic clouds using conventional techniques employing the magnetic field and bulk plasma properties.

ICME1 (DOYs 194–195) drives a shock midday on DOY 193 prior to the interval studied here. Energetic ion intensities at the start of DOY 194 remain elevated

above background. ICME1 contains an evolved cloud with internal pressure comparable to the adjacent plasma and little velocity gradient, indicating it is nearly fully expanded.

ICME2 (DOYs 195–196) does not contain a cloud, and the ionic composition is consistent with typical slow solar wind sources. While ICMEs are sometimes thought of as fast objects, the 600 km s^{-1} speed of this transient is lower than nominal fast wind conditions and it has the composition of a slow wind. The upstream shock S2 is moderately strong and quasi-perpendicular. Shock accelerated 0.5–1.0 MeV protons are observed with corresponding intensity increase in 0.5–2.0 MeV nucl^{-1} He, CNO, and Fe. The O increase continues to 13 MeV nucl^{-1}. Intensity increases in Si and Fe at similar energies are suggested, but somewhat obscured by the presence of galactic cosmic rays. The presence of highly ionized Fe above 0.2 MeV nucl^{-1} and ^{3}He enrichments above 0.5 MeV nucl^{-1} indicate that both S1 and S2 reaccelerated remnant impulsive SEP material.

ICME3 (DOYs 196–197) contains a second moderately evolved cloud with a greater velocity gradient and elevated average wind speed. The ejecta shows an enhanced He/H ratio and thermal C, O, and Fe charge states indicating ~ 3 MK electron temperatures for the source region. This slightly faster moving ICME shows composition signatures consistent with many magnetic clouds. Although the average wind speed is high, the upstream shock is relatively weak and an inefficient accelerator.

ICME4 (DOYs 197–200) contains a young and unevolved magnetic cloud with strong velocity gradients and elevated magnetic pressure. This object is still expanding. The wind speed is > 1100 km s^{-1} and the southward component of the IMF falls below -51 nT, providing ideal conditions for reconnection at the magnetosphere. Again, the He/H ratio for thermal ions is enhanced, the Fe charge state is elevated, and the inferred electron temperature at the source is ~ 3 MK. Unlike the earlier ejecta, this object shows depleted Fe/O abundances in the thermal population. The shock S4 driven by this ejecta is very strong. Locally accelerated ions are evident up to 2.0 MeV nucl^{-1} at the time the shock passes ACE. Whether the shock at this point is still strong enough to accelerate higher energy ions is difficult to ascertain because of the already high intensities of SEP ions. Abundances of heavier or higher rigidity ions < 2.0 MeV nucl^{-1} such as Fe are substantially enhanced compared with lighter or lower rigidity ions like ^{4}He.

Overarching the energetic particle observations at the shocks is the presence of prolonged SEP populations apparently resulting from several solar sources. Two major increases in 0.038–0.315 MeV electron intensity were observed. The first begins 194/20:25 UT and is well correlated with various solar electromagnetic signatures occurring at west 65°. The second arrives 196/10:39 UT and is clearly associated with the Bastille Day event even though the location of the electromagnetic signatures were at west 7°. The prompt arrival of the near-relativistic electrons may indicate that the orientation of the IMF in the inner heliosphere at the time of the Bastille Day flare is not well described by a traditional spiral.

This possibility is supported by the MAG observations of a highly non-spiral IMF during the following 2 days. It is equally likely that these observations suggest the energetic electrons are accelerated by a shock of large longitudinal extent and that the flare region is not the acceleration point for the particles. The acceleration region may span a wide range of heliographic longitudes.

With the arrival of the first electron event on DOY 194, ACE observes 0.25–0.54 MeV nucl^{-1} SEP Fe with high charge states and a high Fe/O ratio apparently originating in an active region and accelerated by flare-related processes. The period between the clouds on DOYs 194 and 197 contain no evidence of a mixture of gradual and impulsive events, suggesting that the interplanetary medium was sufficiently disturbed during this time to disrupt the magnetic connection between the Earth and the western active regions. After DOY 197, the SEP charge state and elemental composition was more consistent with a mixture of two acceleration sources.

Only the Bastille Day event produced significant SEP ion enhancements at > 10 MeV nucl^{-1}. Although this was the largest SEP event yet of the current solar cycle at these energies, in many ways it was unremarkable. Both the elemental and isotopic abundances are nearly unfractionated relative to average gradual SEP and solar system abundances.

ACE Level-2 validated data are available within three months at the ACE Science Center (http://www.srl.caltech.edu/ACE/ASC/). Preliminary Browse data is available within 3 days. Continuous, real-time solar wind monitoring is provided for monitoring and prediction purposes only (http://sec.noaa.gov/ace/ACErtsw_home.html) within 5 minutes of the measurement.

Appendix. Flare Times

To aid in the discussion of ACE observations, we present in Table IV a listing of Hα flares and associated X-ray flares obtained from *Solar-Geophysical Data* that may have relevance to the ACE data. Only flares with importance above subflare are included. We include only X-ray events that came from the same active region as was identified for the Hα flare and only those where the start time of the X-ray was within ~ 30 min of the start time of the Hα flare. We refrain from associating shocks and ICMEs with specific flare events.

Acknowledgements

TABLE IV

Flare times[a,b]

Day	Hr:min (UT)	Hα location	Hα imp.	X-ray class
190	07:32	N17 W07	1N	
190	13:21	N17 W08	1F	C3.1
191	07:18	N16 E72	1N	M5.7
191	08:22	N19 W17	1F	
192	13:55	N18 E52	1N	M1.4
192	18:32	S18 W32	1N	M1.8
192	21:32	N18 E49	2B	M5.7
193	13:20	N18 E27	2N	
193	18:49	N16 W56	1N	M1.1
194	04:54	N16 E31	1N	M1.2
194	10:15	N17 E27	2B	X1.9
194	18:48	N16 W64	2F	M5.7
194	20:13	N17 W65	SF[c]	
195	16:05	N13 E65	1N	M1.1
195	16:16	N19 W75	1F	M1.5
195	17:52	N19 W82	1N	
195	18:46	N18 E08	1F	M1.2
196	08:09	N14 E53	1F	
196	10:21	N22 W07	3B	X5.7
196	10:53	N17 E01	2B	
196	13:46	N20 W08	1N	M3.7
197	05:55	S09 W13	1F	
198	01:22	S11 E53	1N	C6.3
198	02:05	N09 E81	1N	
198	19:36	S13 E48	1N	C6.5
198	20:46	S04 E68	1N	C4.9
198	21:49	N14 E76	1N	M1.1
198	23:41	N17 W38	2F	M1.4
199	08:30	S10 E36	1F	C5.3
199	13:37	S08 E31	1F	M1.2
199	18:06	N19 W47	1F	
199	20:16	S11 E36	1N	M2.4
199	22:31	S12 E30	1F	

[a]Obtained from *Solar-Geophysical Data*.
[b]Only Hα flares with importance above subflare.
[c]One subflare included for electron timing.

References

Anders, E. and Grevesse, N.: 1989, *Geochim. Cosmochim. Acta* **53**, 197.

Aulaner, G., DeLuca, E. E., Antiochos, S. K., McMullen, R. A., and Golub, L.: 2000, *Astrophys. J.* **540**, 1126.

Borrini, G., Gosling, J. T., Bame, S. J., and Feldman, W. C.: 1982, *J. Geophys. Res.* **87**, 7370.

Breneman, H. H. and Stone, E. C.: 1985, *Astrophys. J.* **299**, L57.

Burlaga, L. F., Skoug, R. M., Smith, C. W., Webb, D. F., Zurbuchen, T. H., and Reinard, A.: 2001, *J. Geophys. Res.*, in press.

Desai, M. I., Mason, G. M., Dwyer, J. R., Mazur, J. E., Smith, C. W., and Skoug, R. M.: 2001, *Astrophys. J.* **553**, L89.

Gloeckler, G. and Geiss, J.: 1998, *Space Sci. Rev.* **84**, 275.

Gloeckler, G., Krimigis, S. M., Hawkins, S. E., Haggerty, D. K., Lohr, D. A., Fiore, E., Armstrong, T. P., Holland, G., Lanzerotti, L. J.: 1998, *Space Sci. Rev.* **86**, 497.

Gold, R. E. *et al.*: 1998, *Space Sci. Rev.* **86**, 541.

Gosling, J. G., Pizzo, V., and Bame, S. J.: 1973, *J. Geophys. Res.* **78**, 2001.

Gosling, J. T., Baker, D. N., Bame, S. J., Feldman, W. C., Zwickl, R. D., and Smith, E. J.: 1987, *J. Geophys. Res.* **92**, 8519.

Henke, T. *et al.*: 1998, *Geophys. Res. Lett.* **25**, 3465.

Jordanova, V. K., Thorne, R. M., Farrugia, C. J., Dotan, Y., Fennel, J. F., Thomsen, M. F., Reeves, G. D., and McComas, D. J.: 2001, *Solar Phys.*, this issue.

Klecker, B.: 2001, in R.A. Mewaldt *et al.* (eds.), *Acceleration and Transport of Energetic Particles in the Heliosphere*, ACE 2000 Symposium, AIP, p. 139.

Kosovichev, A. G. and Zharkova, V. V.: 2001, *Astrophys. J.* **550**, L105.

Lepping, R. P., Berdichevsky, D. B., Burlaga, L. F., Lazarus, A. J., Kasper, J., Desch, M. D., Wu, C. C., Reames, D. V., Singer, H. J., Smith, C. W., and Ackerson, K.: 2001, *Solar Phys.*, this issue.

Lepri, S., Zurbuchen, T. H., Fisk, L. A., Richardson, I. G., Cane, H. V., and Gloeckler, G.: 2001, *J. Geophys. Res.*, in press.

Leske, R. A., Mewaldt, R. A., Cohen, C. M. S., Cummings, A. C., Stone, E. C., Wiedenbeck, M. E., Christian, E. R., and von Rosenvinge, T. T.: 1999, *Geophys. Res. Lett.* **26**, 2693.

Mason, G. M., Mazur, J. E., and Dwyer, J. R.: 1999, *Astrophys. J.* **525**, L133.

Mason, G. M., Gold, R. E., Krimigis, S. M., Mazur, J. E., Andrews, G. B., *et al.*: 1998, *Space Sci. Rev.* **86**, 409.

Mason, G. M. *et al.*: 1999, *Geophys. Res. Lett.* **26**, 141.

Mazur, J. E., Mason, G. M., Klecker, B., McGuire, R. E.: 1993, *Astrophys. J.* **404**, 810.

Mazur, J. E., Mason, G. M., Looper, M. D., Leske, R. A., and Mewaldt, R. A.: 1999, *Geophys. Res. Lett.* **26**, 173.

McComas, D. J., Bame, S. J., Barker, P., Feldman, W. C., Phillips, J. L., Riley, P., and Griffee, J. W.: 1998, *Space Sci. Rev.* **86**, 563.

Mitchell, D. G., Hsieh, K. C., Curtis, C. C., Hamilton, D. C., Voss, H. D., Roelof, E. C., and C:son Brandt, P.: 2001, *Geophys. Res. Lett.* **28**, 1151.

Möbius, E. *et al.*: 1998, *Space Sci. Rev.* **86**, 449.

Möbius, E., Popecki, M., Klecker, B., Kistler, L. M., Bogdanov, A., Galvin, A. B., Heirtzler, D., Hovestadt, D., Lund, E. J., Morris, D., and Schmidt, W. K. H.: 1999, *Geophys. Res. Lett.* **26**, 145.

Ng, C. K., Reames, D. V., and Tylka, A. J.: 1999, *Geophys. Res. Lett.* **26**, 2145.

Osherovich, V., and Burlaga, L. F.: 1997, in Crooker, N., Joselyn, J. A., and Feynman, J. (eds.), *Coronal Mass Ejections*, AGU Geophysical Monograph 99, AGU, Washington, DC, p. 157.

Osherovich, V. A., Farrugia, C. J., and Burlaga, L. F.: 1993, *Adv. Space Res.* **13**, 57.

Parker, E. N.: 1963, *Interplanetary Dynamical Processes*, Wiley-Interscience, New York.

Reames, D. V.: 1990, *Astrophys. J.* **358**, L63.

Reames, D. V.: 1999, *Space Sci. Rev.* **90**, 413.

Reames, D. V. *et al.*: 2001, 'Solar Energetic Particles and Space Weather', *Proceedings of the Space Technology and Applications International Forum*, February 11–February 14, 2001, New Mexico.

Reames, D. V., Ng, C. K., and Tylka, A. J.: 2001, *Astrophys. J.* **548**, L233.

Skoug, R. M., Feldman, W. C., Gosling, J. T., McComas, D. J., and Smith, C. W.: 2000, *J. Geophys. Res.* **105**, 23,069.

Smith, C. W., Acuña, M. H., Burlaga, L. F., L'Heureux, J., Ness, N. F., and Scheifele, J.: 1998, *Space Sci. Rev.* **86**, 613.

Stone, E. C., Frandsen, A. M., Mewaldt, R. A., Christian, E. R., Margolies, D., Ormes, J. F., and Snow, F.: 1998a, *Space Sci. Rev.* **86**, 1.

Stone, E. C., Cohen, C. M. S., Cook, W. R., Cummings, A. C., Gauld, B., Kecman, B., Leske, R. A., Mewaldt, R. A., Thayer, M. R., Dougherty, B. L., Grumm, R. L., Milliken, B. D., Radocinski, R. G., Wiedenbeck, M. E., Christian, E. R., Shuman, S., and von Rosenvinge, T. T.: 1998b, *Space Sci. Rev.* **86**, 357.

Tylka, A. J., Reames, D. V., and Ng, C. K.: 1999, *Geophys. Res. Lett.* **26**, 2141.

Tylka, A. J., Boberg, P. R., McGuire, R. E., Ng, C. K., and Reames, D. V.: 2001, in R. A. Mewaldt *et al.* (eds.), *Acceleration and Transport of Energetic Particles Observed in the Heliosphere: ACE 2000 Symposium*, AIP, p. 147.

von Steiger, R., Geiss, J., and Gloeckler, G.: 1997, in J. R. Jokipii, C. P., Sonett, and M. S. Giampapa (eds.), *Cosmic Wind and the Heliosphere*, University of Arizona Press, p. 581.

Zurbuchen, T. H., Hefti, S., Fisk, L. A., Gloeckler, G., and Schwadron, N. A.: 2000, *J. Geophys. Res.* **105**, 18,327.

Zwickl, R. D., Asbridge, J. R., Bame, S. J., Feldman, W. C., and Gosling, J. T.: 1983, in M. Neugebauer (ed.), *NASA Conf. Publ.* **CP-2280**, 711.